Carnegie Observatories Astrophysics Series, Vol. 3:
Clusters of Galaxies: Probes of Cosmological Structure and Galaxy Evolution, 2004
ed. J. S. Mulchaey, A. Dressler, and A. Oemler (Cambridge: Cambridge Univ. Press)

Galaxy Clusters as Probes of Cosmology and Astrophysics

AUGUST E. EVRARD
Departments of Physics and Astronomy, Michigan Center for Theoretical Physics, University of Michigan

Abstract

Clusters of galaxies emerge as nodes in the gravitationally evolving cosmic web of dark matter and baryons that defines the large-scale structure of the Universe. X-ray and optical observations offer plentiful evidence of clusters' dynamical youth, yet bulk measures derived from these observations are tightly correlated, indicating a high degree of structural regularity that makes the population an attractive probe of cosmology. Accurate constraints on cosmological parameters require a precise and unbiased model relating observables to total mass, as well as a statistical characterization of the massive halo population within a given cosmology. In this contribution, I focus on the latter by providing evidence from simulations for $\mathcal{O}(10\%)$ calibration of the space density as a function of mass and for $\mathcal{O}(1\%)$ calibration of the dark matter virial relation. Matching the observed space density as a function of X-ray temperature for a ΛCDM world model is presented as an example of astrophysical/cosmological confusion. The resulting constraint $\beta\,\sigma_8{}^{-5/3} = (1.10 \pm 0.07)$ combines β, the ratio of specific energies in dark matter and intracluster gas, with σ_8, the normalization of the mass fluctuation spectrum. Disentangling astrophysical and cosmological factors for upcoming large statistical surveys is the main challenge in the quest to use galaxy clusters as sensitive probes of dark matter and dark energy.

1.1 Introduction

Cosmology is now a data-rich subject, with empirical support from at least four independent channels: the cosmic microwave background (CMB) radiation, light element nucleosynthesis, Type Ia supernovae, and large-scale cosmic structure. The latest CMB observations from the *Wilkinson Microwave Anisotropy Probe* (*WMAP*; Bennett et al. 2003) and ground-based experiments have revealed the series of acoustic peaks expected in an inflationary, hot Big Bang picture (Scott, Silk, & White 1995) and spotlight a fundamentally unexpected model containing roughly two-thirds vacuum or dark energy, one-third dark matter, and about four percent ordinary (baryonic) matter (Spergel et al. 2003). The nature of the principal dark components remains a mystery.

The ornery energy of Fritz Zwicky, though unlikely to dominate the Universe, is nonetheless involved in all this. Zwicky's revelation of dark matter in the Coma cluster (Zwicky 1933, 1937) established the roots of the modern era, and it is fitting to recognize his seminal contributions at this centennial event of the Carnegie Observatories. The problem of *missing mass*, as it was then known, derived from the humble virial theorem, helped to spark the

Table 1.1. *Mass Hierarchy in the Coma Cluster*

Component	$M(< 1.5\,h^{-1}$ Mpc) $(M_\odot)$	$M/M_{\rm vis}$
Total[a]	$1.3 \pm 0.3 \times 10^{15}\ h_{70}^{-1}$	9.0 ± 2.5
Intracluster gas	$1.3 \pm 0.2 \times 10^{14}\ {h_{70}}^{-5/2}$	0.90 ± 0.02
Galaxies	$1.4 \pm 0.3 \times 10^{13}\ h_{70}^{-1}$	0.10 ± 0.03

[a]Estimated from gas dynamic simulations.

now vast and complex hunt at large collider experiments and underground laboratories for the particle constituent of dark matter.

A half-century after Zwicky's study, advances in X-ray astronomy revealed the full mass hierarchy within clusters: galaxies are outweighed by an encompassing hot intracluster medium (ICM), and the combined visible mass remains a minority of the total. High-throughput spectroscopy of the ICM established its nearly isothermal nature, and high-resolution imaging from the *ROSAT* mission (Briel, Henry, & Böhringer 1992) enabled accurate estimates of ICM masses as well as estimates of total masses, under a hydrostatic equilibrium assumption, which confirmed, within $\sim 30\%$ statistical errors, the optical virial estimates of Dressler (1978) and many others (see Girardi et al. 2000). Estimates of the mass hierarchy for the Coma cluster (White et al. 1993) are listed in Table 1.1 for a Hubble constant $H_0 = 70\,h_{70}$ km s^{-1} Mpc^{-1}.

Why was galaxy formation in Coma so inefficient? To what extent is the environment within Coma representative of the state of clusters in general? Or of the Universe as a whole? Answers to many of these questions are now becoming available from increasingly large statistical surveys of galaxies and clusters, along with detailed investigation of individual clusters using 8 m-class optical telescopes. Papers presented at this meeting offer many excellent examples of both such approaches.

On the theory side, modeling the development of galaxies and the ICM within a cosmological framework of hierarchical clustering poses a formidable task. Although the physical processes—gravity, heating by shocks, cooling and (especially in low-density regions) heating by radiation, magnetic fields, conduction, turbulent mixing, etc.—are now firmly in hand, the complex, nonlinear interactions that govern their time evolution are analytically intractable, even for highly simplified geometries. Computational solutions are progressing (Kauffman et al. 1999; Somerville & Primack 1999; Cole et al. 2000), but the accuracy of solutions is limited by uncertainties associated with the "mesoscopic" processes involved in stellar birth, evolution, and death. The role of central black holes/active galactic nuclei on the galaxy/ICM interaction is only beginning to be explored (cf. Brüggen & Kaiser 2002).

Such modeling uncertainties are a cause for concern to cosmologists, since biased parameter estimates will result from application of an incorrect astrophysical model. Let $\mathcal{C}$ represent the vector of cosmological parameters (clustered mass density $\Omega_{\rm m}$, baryon mass density $\Omega_{\rm b}$, vacuum energy density Ω_Λ or dark energy $\Omega_{\rm DE}$, spectrum normalization σ_8, etc.) and let $\mathcal{R}$ represent a set of observations from a cluster survey. Then Bayes' theorem makes clear that identifying the most likely cosmology is dependent on knowing precisely how likely are the observations within that world model:

$$p(\mathcal{C} \mid \mathcal{R}) \propto p(\mathcal{R} \mid \mathcal{C})\, p_{\rm prior}(\mathcal{C}). \tag{1.1}$$

For the CMB, the relevant likelihoods $p(\mathcal{R} \mid \mathcal{C})$ are calculable to high accuracy with codes such as CMBFAST (Seljak & Zaldarriaga 1996). For Type Ia supernovae, only the luminosity distance $d_L(z)$ is needed to compute the apparent brightness of standard candles as a function of redshift (although proving the standard candle nature is challenging). For galaxy clusters and most other large-scale structure signatures, nonlinear dynamics and astrophysical uncertainties complicate the computation of the observable likelihood $p(\mathcal{R} \mid \mathcal{C})$.

There are computational and empirical reasons to suspect that the problem, though complex, is still tractable. Tight correlations, such as that between ICM mass $M_{\rm ICM}$ and X-ray temperature $T_{\rm X}$ (Mohr, Mathiesen, & Evrard 1999), are observed among intrinsic properties of local clusters. Simulated clusters follow narrow scaling relations (Evrard 1989; Navarro, Frenk, & White 1995, hereafter NFW; Evrard, Metzler, & Navarro 1996; Bryan & Norman 1998). These findings motivate a basic framework in which clusters are essentially a one-parameter family ordered by a size parameter, typically taken to be the total mass M. (Exactly how mass is defined is a detail discussed below.) Tight scaling relations between M and $T_{\rm X}$ reflect virial equilibrium, while retention of the cosmic baryon fraction and inefficient cooling/star formation within cluster environments lead to a strong correlation $M_{\rm ICM} \sim (\Omega_{\rm b}/\Omega_{\rm m}) f_{\rm hot} M$, with $f_{\rm hot}$ the fraction of baryons not processed into cold gas or stars.

In this paper, I take the perspective of separating the problem into two, quasi-independent pieces. For a given cosmology, the question of computing the likelihood of an observable, say the expected number of clusters with temperate T at redshift z, can be split into two parts, namely

- How many clusters of mass M exist in this cosmology at redshift z?
- What is the likelihood that a cluster of mass M at redshift z will have temperature T?

In general, the answer to the second question will require an astrophysical model defined by some set of parameters $\mathcal{A}$. For example, varying the efficiency of supernova or active galactic nuclei heating will affect the detailed form of the joint likelihood $p(M,T)$ at a particular epoch.

Under this separable assumption, the likelihood of forming a cluster of temperature T at redshift z will be a convolution

$$p(T,z|\mathcal{C},\mathcal{A}) = \frac{\int dM\; p(M,z|\mathcal{C})\; p(T\,|M,z,\mathcal{A})}{\int dM\; p(M,z|\mathcal{C})}, \tag{1.2}$$

where $p(M,z|\mathcal{C})$ gives the likelihood that a cluster of mass M exists at redshift z in cosmology $\mathcal{C}$ and $p(T\,|M,z,\mathcal{A})$ gives the likelihood that such a cluster has temperature T for the particular astrophysical model $\mathcal{A}$.

In § 1.2, after briefly reviewing the framework of nonlinear structure formation, I present recent calibrations of the cluster space density by large simulations and show that this problem, modulo some inherent arbitrariness in assigning mass to halos, is now on quite firm footing. In § 1.3, the virial relation linking mass to ICM temperature is discussed and discrepancies between computational and empirical approaches are noted. This motivates a "back-door" approach to calibrating the mass scale of the cluster population that stems from very precise determination of the dark matter virial relation discussed in § 1.4. Implications emerge in § 1.5, where the observed cluster space density as a function of temperature forges a link between σ_8 (a cosmological parameter) and the ratio of cluster component energies β (a purely astrophysical parameter). Unless sources of substantial systematic error can be identified, the low normalization $\sigma_8 \approx 0.7-0.8$ inferred from *WMAP* analysis will require significantly more heating of the ICM plasma than is provided by gravitational collapse alone. A concluding discussion is provided in § 1.6.

1.2 Clusters as Dark Matter Potential Wells

An early inflationary period in the history of the Universe is thought to seed the Universe with fluctuations in energy density (Kolb & Turner 1990). Depending on the chosen scenario, the spectrum of primordial density fluctuations can differ from a power law, and a general expression is a form with a running spectral index:

$$P_{\rm prim}(k) \;=\; P(k_0)\left(\frac{k}{k_0}\right)^{n_s(k)}, \tag{1.3}$$

where $n_s(k) = n_s(k_0) + dn_s/d\ln k \ln(k/k_0)$. Recent analysis of *WMAP* thermal fluctuations combined with 2dF galaxy and Lyα forest power spectrum estimates suggest, at the 2σ level, a nonzero value for the spectral index derivative $dn_s/d\ln k = -0.031^{+0.016}_{-0.017}$ (Spergel et al. 2003).

During the pre-recombination era, when fluctuation amplitudes are small and a linear treatment of independent wavemodes is valid, the primordial matter perturbations undergo stagnant growth on small scales and (for warm/hot components) strong damping due to free-streaming. The net result of such physics, which is particularly sensitive to the matter density $\Omega_{\rm m}$ and the baryon fraction $\Omega_{\rm b}/\Omega_{\rm m}$, is summarized by a transfer function $T(k)$ that defines the post-recombination power spectrum $P_{\rm rec}(k) \equiv T^2(k) P_{\rm prim}(k)$ (Bond & Efstathiou 1984).

As discussed below, the mass dependence of the cluster space density is sensitive to the logarithmic slope of the linear, post-recombination spectrum $n_{\rm eff} = d\ln P_{\rm rec}(k)/d\ln k$ on $\sim 10\,h^{-1}$ Mpc scales. A statistically precise measurement of $n_{\rm eff}(k)$ can be sought using upcoming large cluster samples, after systematic selection and projection effects are addressed and understood.

1.2.1 Nonlinear Gravitational Condensation

In the linear regime, the growth rate of the fluctuation amplitude at any wavenumber is controlled by a function $D(a)$, the form of which is determined by the mix of matter and energy components in the Universe (Peebles 1980; Carroll, Press, & Turner 1992). As linearized wave amplitudes δ approach unity, mode coupling becomes important, and the linear treatment must be extended to second and higher order (Bernadeau et al. 2002). Comparison with N-body simulations confirm the validity of calculations to tenth order and higher (Szapudi et al. 2000), but precise solution of the deeply nonlinear ($\delta \gtrsim 10^2$) evolution of the matter density and velocity fields is exclusively achieved by numerical simulation (Bertschinger 1998).

Simulations of large comoving volumes show that, as mode-coupling strengthens, the density field develops the texture of a "cosmic web" (Bond, Kofman, & Pogosian 1996), an example of which is shown in Figure 1.1. Filaments and walls surround lower density voids and bound ellipsoidal structures—the halos/clusters housing astrophysical objects—develop through gravitational collapse, with the largest and rarest clusters forming at nodes defined by major filament intersections. As discussed below, the spectrum of halos sizes can be

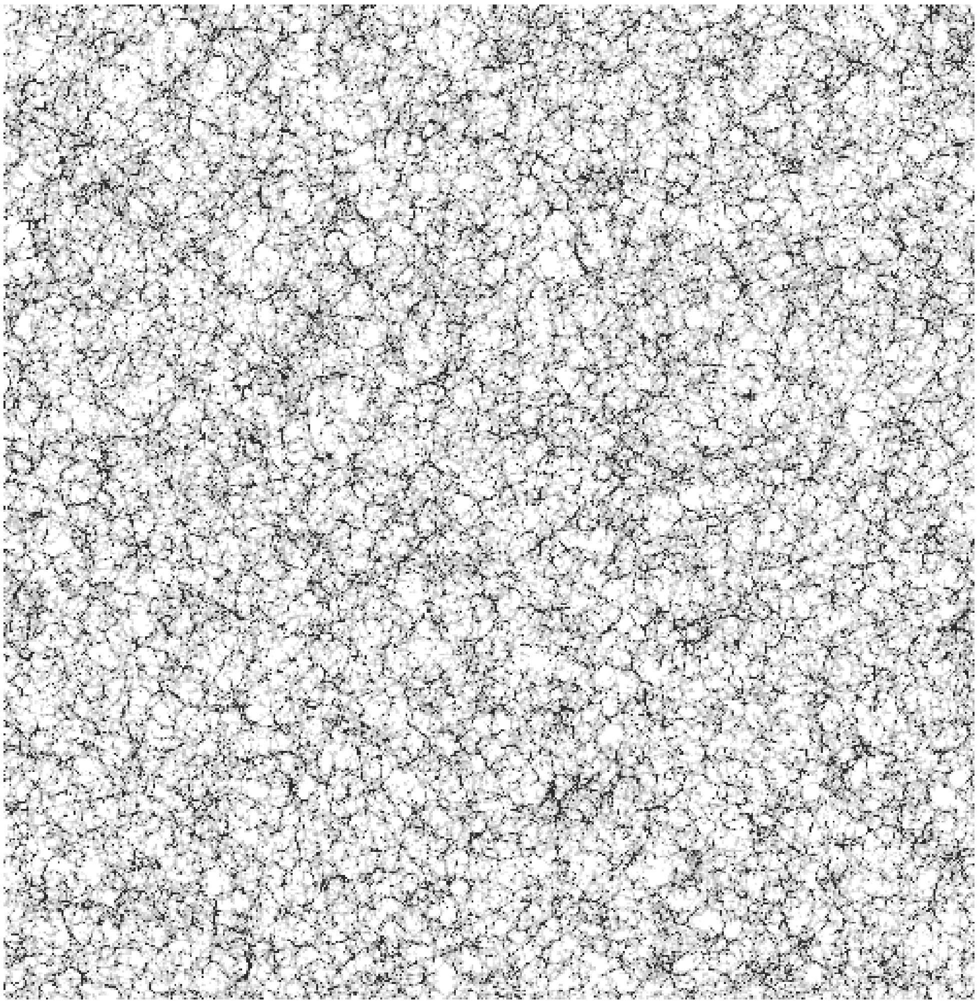

Fig. 1.1. Large-scale structure of cold dark matter in a Hubble Length ($3000\,h^{-1}$ Mpc) slice through a simulated ΛCDM Universe at $z = 0$ (Evrard et al. 2002). The slice thickness with $30\,h^{-1}$ Mpc and the greyscale show regions with above-average density smoothed on a $10^{13}\,h^{-1}M_{\odot}$ scale.

derived analytically from $P_{\rm rec}(k)$ under spherical or ellipsoidal evolution approximations. For effectively power-law spectra, the characteristic mass scale M_* of the distribution evolves in redshift according to $M_*(a) \propto [D(a)]^{6/(n_{\rm eff}+3)}$ (Kaiser 1986), and this feature is the basis for deducing a low matter density Universe from the sky surface density of massive clusters at $z \approx 0.5-1$ (Bahcall & Fan 1998; Donahue et al. 1998; Borgani et al. 2001).

Since both the Gaussian random initial conditions and the process of gravitational amplification have no sharp intrinsic scales, clusters do not develop obvious physical boundaries. Instead, a roughly hydrostatic and dynamically older core connects seamlessly to an infall region fed by material drawn mainly from the embedding filaments. Accretion of small halos occurs nearly continuously up to the present, and major mergers that cause significant phase space rearrangement happen stochastically every few dynamical times. Due to this complexity, a unique definition of cluster mass is hard to justify. Instead, a few, quite similar measures are in common use (Lacey & Cole 1994; White 2001, and references therein), each defined by a threshold density that attempts to separate the quasi-equilibrium, or "virialized", cluster interior from its surrounding, infalling streams.

One way to address the mass ambiguity is to consider the relative merits of different measures. What "added value" does each bring to descriptive analysis of the cluster population? As shown below, it appears that masses set by thresholds defined relative to the *mean* matter density $\rho_{\rm m}(a)$ are convenient for counting clusters, while those defined relative to the critical density $\rho_{\rm c}(a)$ are advantageous for addressing internal structure issues such as the virial relation linking mass to dark matter velocity dispersion or ICM thermal temperature.

In spherical models of perturbation evolution (Gunn & Gott 1972; Bertschinger 1985; Lokas & Hoffmann 2000), a cluster develops from a local peak in the linear density field. Peaks in Gaussian random fields exist on a wide range of scales, so to select those at a particular scale $M \propto R^3$ it is useful to smooth the continuous density field $\rho(x)$ with a spatial filter $W(|x'-x|/R)$. The variance in the smoothed density field is

$$\sigma^2(M) \;=\; \frac{1}{(2\pi)^3}\int d^3k\, P_{\rm rec}(k)\, \hat{W}^2(kR), \tag{1.4}$$

where $\hat{W}(kR)$ is the Fourier transform of the spatial filter function. The use of a spherical Heaviside, or "top-hat," function $[W(r/R) \equiv 1$ for $r/R \leq 1$ and 0 otherwise] with comoving scale $8\,h^{-1}$ Mpc defines a conventional measure of the present, linearly evolved power spectrum amplitude $\sigma_8 \equiv \sigma(M_8)$, with $M_8 = 1.785(\Omega_{\rm m}/0.3) \times 10^{14} h^{-1} M_\odot$. The probability density function (PDF) of the filtered density field is Gaussian normal in the variable $\nu \equiv \delta/\sigma(M)$.

1.2.2 The Cluster Space Density

Counting the number of clusters as a function of size is currently an inexact exercise for observers and theorists alike. In the sky, optical/infrared catalogs can be searched for galaxy concentrations in redshift/color space (Bahcall et al. 2003; Nichol 2004). Detection of the ICM via its X-ray emission (Rosati, Borgani, & Norman 2002) or its spectral distortion of the microwave background radiation (Carlstrom, Holder, & Reese 2002) is another means of cluster identification. Although the observable signatures are strongly correlated (to first order, via the ever-useful "bigger is bigger" maxim), the scaling relations linking pairs of observables display typically tens of percent intrinsic scatter (Borgani et al. 1999; Mohr et al. 1999; Sanderson et al. 2003), and each measure is subject to different sources of systematic and random errors.

The upshot is that an X-ray temperature-limited sample of clusters will differ somewhat from an optical richness-limited sample, and both will differ to some degree with an Sunyaev-Zel'dovich-limited set of clusters. Given enough signal-to-noise ratio, the most massive clusters will be identified by any method, but differences in how projected signals add, along with intrinsic scatter among observables, will, at the minimum reorder, and more likely reorder and blend a set of objects detected at even high signal-to-noise ratio. Under realistic conditions, confusion will become more severe as one pushes to smaller systems near the sample detection threshold (Bahcall et al. 2003).

With the advantage of full spatial information, theorists working with simulated volumes are afforded higher precision. For a point set of simulation particles, percolation methods, such as the "friends-of-friends" algorithm of Davis et al. (1985), have been a popular way to define halos. Complex geometries typically bound the objects defined with this method (see Fig. 4 of White 2001), and this aspect can complicate attempts to connect this mass measure to observations.

A geometrically simpler approach is to identify a cluster as material lying within a sphere, centered on a local density maximum or potential minimum, whose radial extent r_Δ is defined by an enclosed isodensity condition $M(< r_\Delta)/(4\pi {r_\Delta}^3/3) = \rho_t(z)$. Such spherical overdensity (SO) masses require a choice of threshold density $\rho_t(z)$ that is typically written as a multiple Δ of either the mean mass density $\rho_m(z)$ or the critical density $\rho_c(z)$. These measures are referred to as "mean" and "critical" masses below. Although many treatments employ a time-varying Δ in cosmologies with $\Omega_m \neq 1$ (Eke, Cole, & Frenk 1996), evidence below suggests that this complication is unnecessary, and Δ here is assumed constant.

Given a mass measure M, the space density $n(M,z|\mathcal{C})$, or *mass function*, describes the probability of finding a cluster at redshift z with total mass in the interval M to $Me^{\mathrm{d}\ln M}$ within a suitably small comoving volume element dV:

$$p(M,z|\mathcal{C}) \;=\; n(M,z|\mathcal{C})\,dV. \tag{1.5}$$

An analytic form for the mass function, based on spherical dynamics and a Gaussian random density field, was first developed by Press & Schechter (1974, hereafter PS) and rederived using a rigorous excursion set approach by Bond et al. (1991). The resulting shape of $n(M,z)$ is dictated by the linear power spectrum $\sigma(M)$ and its logarithmic derivative. The mass fraction in halos of mass M at redshift z can be expressed in terms of a single function $f(\sigma^{-1})$:*

$$f(\sigma^{-1},z) \;\equiv\; \frac{M}{\rho_m(z)}\; n(M,z)\; \frac{\mathrm{d}\ln M}{\mathrm{d}\ln \sigma^{-1}}. \tag{1.6}$$

The dependence on cosmology is implicit, determined by the fluctuation spectrum and its rate of linear evolution $D(a)$.

The PS treatment employs a spherical collapse model that assumes equilibrium is reached when the linearly evolved interior density reaches a critical threshold δ_c (equal to 1.686 in an Einstein-de Sitter cosmology). This leads to a mass function of the form

$$f(\sigma^{-1}) \;=\; \sqrt{2/\pi}\,(\delta_c\sigma^{-1})\,\exp[-(\delta_c\sigma^{-1})^2/2]. \tag{1.7}$$

Initial comparison of the model with N-body simulations yielded good agreement (Efstathiou et al. 1988), but as computational dynamic range and fidelity improved, disagreement in the detailed shape of the mass function emerged. Introduction of ellipsoidal, rather than spherical, perturbation evolution greatly improved agreement with simulations (Sheth & Tormen 1999; Sheth, Mo, & Tormen 2001, hereafter ST). The mass function in this case takes the form

$$f(\sigma^{-1}) \;=\; A_{\mathrm{ST}}\sqrt{2a/\pi}\,[1+(a\delta_c\sigma^{-1})^{-p}]\,(\delta_c\sigma^{-1})\,\exp[-(a\delta_c\sigma^{-1})^2/2], \tag{1.8}$$

with parameters $A_{\mathrm{ST}} = 0.3222$, $a = 0.707$, and $p = 0.3$.

Massively parallel computers, with aggregate memory in excess of one terabyte, have

* Note that, since $\sigma(M)$ is a monotonic decreasing function in cold dark matter models, its inverse $\sigma^{-1}(M)$ has the same sense as mass; high σ^{-1} implies high mass and *vice versa*.

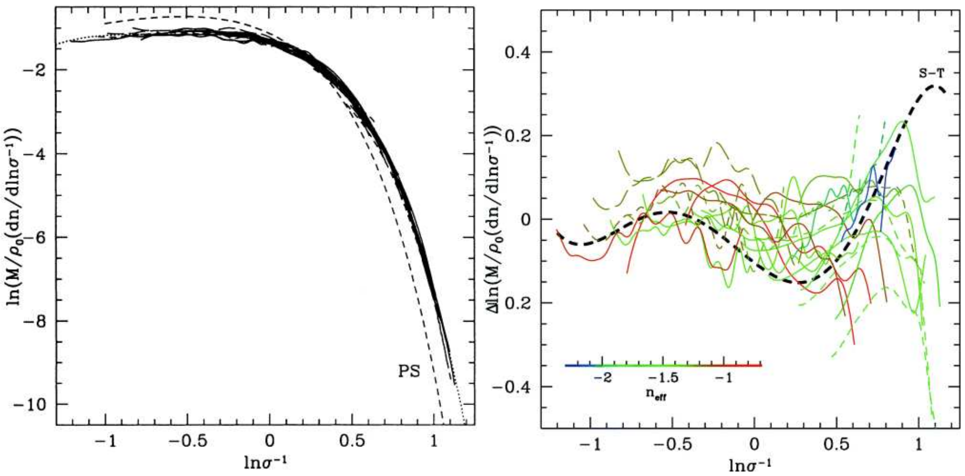

Fig. 1.2. Calibration of the mass function from a set of 29 halo samples extracted from Virgo Consortium simulations (Jenkins et al. 2001). *Left:* Mass fraction in halos as a function of the similarity variable $\sigma^{-1}(M)$. The dotted curve shows the fit to the Jenkins mass function (Eq. 1.9), while the dashed curve shows that the PS expectation (Eq. 1.7) has the wrong shape. *Right:* Residuals in number density between the binned simulated samples and the Jenkins mass function fit are shown as thin lines. The dashed line shows the difference between the Jenkins mass function and ST prediction (Eq. 1.8), with parameters given in the text.

enabled production of very large statistical samples of virtual clusters. Calibrations of the mass function from such samples are reported in a number of recent papers (Governato et al. 1999; Bode et al. 2001; Jenkins et al. 2001; Evrard et al. 2002; Hu & Kratsov 2003; Reed et al. 2003). The results from analysis of a suite of simulations performed by the Virgo Consortium (Jenkins et al. 2001) are shown in Figure 1.2. The mass fraction as a function of $\sigma^{-1}(M)$ is shown for 29 halo samples identified in 13 simulations and covering epochs $z \approx 0-5$ in four different cosmological models (see Table 2 of Jenkins et al. 2001).

All of the models are well fit by a function (hereafter the Jenkins mass function) of the form

$$f(\ln \sigma^{-1}) \;=\; A\;\exp[-|\ln \sigma^{-1} + B|^{\epsilon}]. \tag{1.9}$$

The parameter B controls the location of the peak in the collapsed mass fraction (e^B plays the role of δ_c in the PS and ST forms) while A controls the overall mass fraction in halos and ϵ stretches the function to fit the overall shape of the simulation results. Values $A=0.315$, $B=0.61$, and $\epsilon=3.8$ fit the data in Figure 1.2, which uses a friends-of-friends mass measure with a linking length of 0.2 times the mean interparticle spacing. Note that these parameters are independent of cosmological model and epoch. In this sense, it may be said that Nature prefers to do *accounting* relative to the mean mass density.

We will see below that Nature appears to prefer doing *dynamics* relative to the critical density. For a critical SO(200) mass measure, Evrard et al. (2002) show that Equation (1.9) provides a good fit to the mass function with Ω_m-dependent fit parameters $A(\Omega_m)=0.27-$

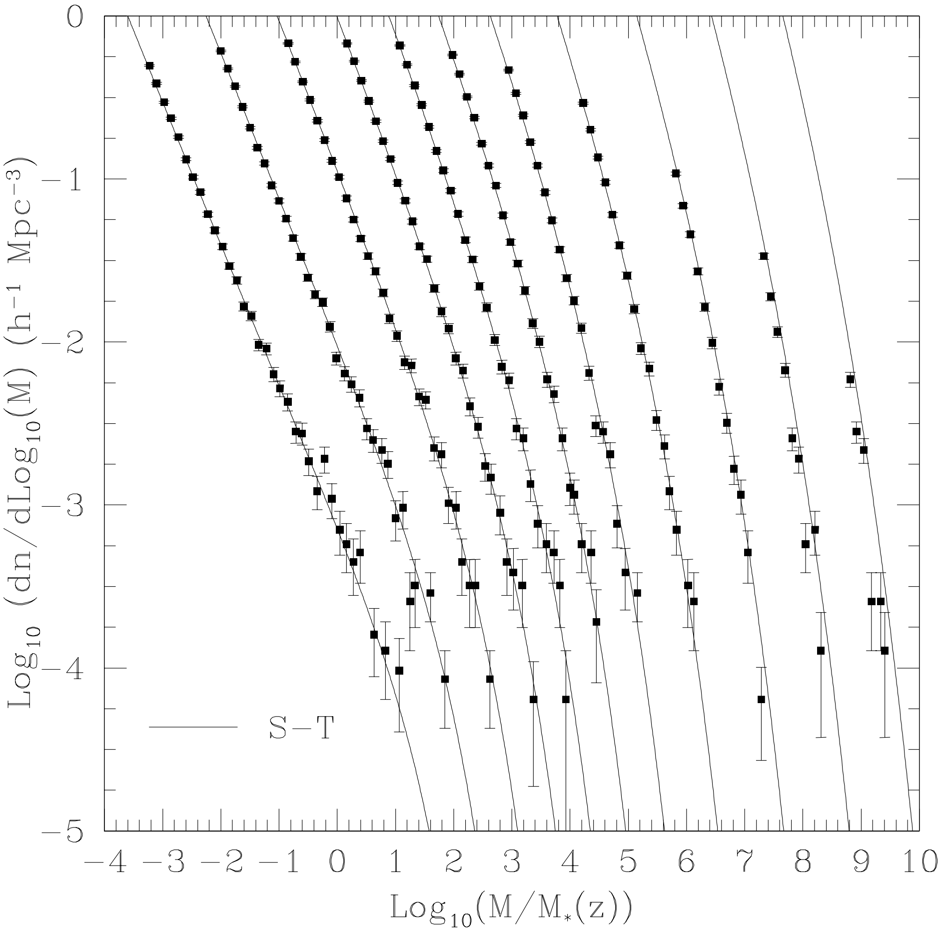

Fig. 1.3. The mass function of halos from the ΛCDM simulation of Reed et al. (2003). Data points with Poisson error bars show the simulation results, while curves are ST predictions at redshifts (from left to right) 0, 1, 2, 3, 4, 5, 6.2, 7.8, 10, 12.1, and 14.5.

$0.07\Omega_m$ and $B(\Omega_m)$=0.65+$0.11\Omega_m$ (and ϵ=3.8). Hu & Kravtsov (2003) provide independent confirmation of this fit for the case Ω_m=0.15.

The right panel of Figure 1.2 shows that this form predicts the space density to an accuracy of $\sim 20\%$. This panel also shows deviations with respect to the ST form with recalibrated parameters A_{ST} = 0.353, a = 0.73, and p=0.175. With the exception of the rarest objects ($\ln \sigma^{-1} \gtrsim 0.7$), this model gives an equally good fit. The PS formula for the rarest systems underpredicts their abundance by more than a factor 10. The use of an ellipsoidal collapse model (with two added parameters calibrated by simulation) is clearly superior to the original PS spherical treatment.

Reed et al. (2003) reach a similar conclusion on the ST predictions, and offer a correction factor to apply at high masses. As shown in Figure 1.3, their 432^3 particle simulation of a

$50\,h^{-1}$ Mpc region, which probes a more shallow region of the power spectrum compared to cluster scales, shows stunning agreement with the ST predictions over a wide dynamic range in number density and epoch. The finding that the fit works well over 10 decades in normalized mass $M/M_*(z)$ is particularly impressive.

1.2.3 Mass-scale Uncertainty and σ_8

The space density of the most massive clusters at a given epoch is exponentially sensitive to σ_8, but extracting σ_8 from observations of massive clusters requires accurate knowledge of cluster masses. From the form of the Jenkins mass function, Evrard et al. (2002) derive $\mathrm{d}\ln\sigma_8/\mathrm{d}\ln M \simeq 0.4$ for massive clusters in a ΛCDM cosmology, meaning that, at fixed spatial abundance, systematic errors of, say, 25% in the mass scale of clusters translate into a systematic uncertainty of 10% in σ_8. A simple demonstration of this effect is given in Figure 1.4. The shapes of the functions, scaled separately in mass or σ_8, are nearly identical over the space density range 10^{-5} to $10^{-10}h^3$ Mpc^{-3}.

In summary, computational modeling now provides $\sim 10\%$-level accurate calibration of the space density $n(M,z)$ for halos spanning the entire observable range of galaxy cluster masses. In this sense, the theoretical situation is in good shape. The hard task remains of relating mass to readily observable properties of clusters.

1.3 Connecting Mass to Observables: Virial Scaling Relations

Since ICM temperatures and galaxy velocity dispersions are directly observable measures of cluster size, the virial theorem, as Zwicky had long ago appreciated, is a natural starting point for establishing an observable-mass connection.

1.3.1 What is the "Virial Mass" of a Cluster?

Since clusters are dynamically evolving within the large-scale cosmic web, some deviation from hydrostatic and virial equilibrium must be expected. Simulations of colliding pairs of clusters show significant departures from hydrostatic equilibrium during major mergers (Roettiger, Burns, & Loken 1996; Ricker & Sarazin 2002), yet simulations of clusters formed from Gaussian random density fields show that the population as a whole adheres to a surprisingly tight virial relation (Evrard 1989; Navarro et al. 1995; Bryan & Norman 1998; Mathiesen & Evrard 2001). These seemingly inconsistent findings can both be true. Major mergers are relatively rare (Bower 1991; Lacey & Cole 1994; Sheth & Tormen 1999), so small departures from equilibrium are statistically far more likely than order unity variations. Furthermore, dynamical relaxation occurs rapidly, essentially on a single crossing time (Peebles 1970), and the net effect is to drive clusters very nearly along the equilibrium relation (Navarro et al. 1995), even during phases of major mergers (see Fig. 14 of Evrard & Gioia 2002).

The virial relation connects the dark matter velocity dispersion $\sigma_{\rm DM}$ and ICM temperature T, both mass-weighted within a sphere of radius r_Δ, to the corresponding SO mass M_Δ via the form

$$\sigma_{\rm DM}{}^2 \;\propto\; (kT/\mu m_p) = \varepsilon\, GM_\Delta/r_\Delta, \tag{1.10}$$

where μ is the mean molecular weight of the ICM, m_p the proton mass, and ε a dimensionless constant that depends primarily on the internal density profile of clusters. For mass defined against the critical density, the right-hand side scales as $[h(z)M_\Delta]^{2/3}$, where

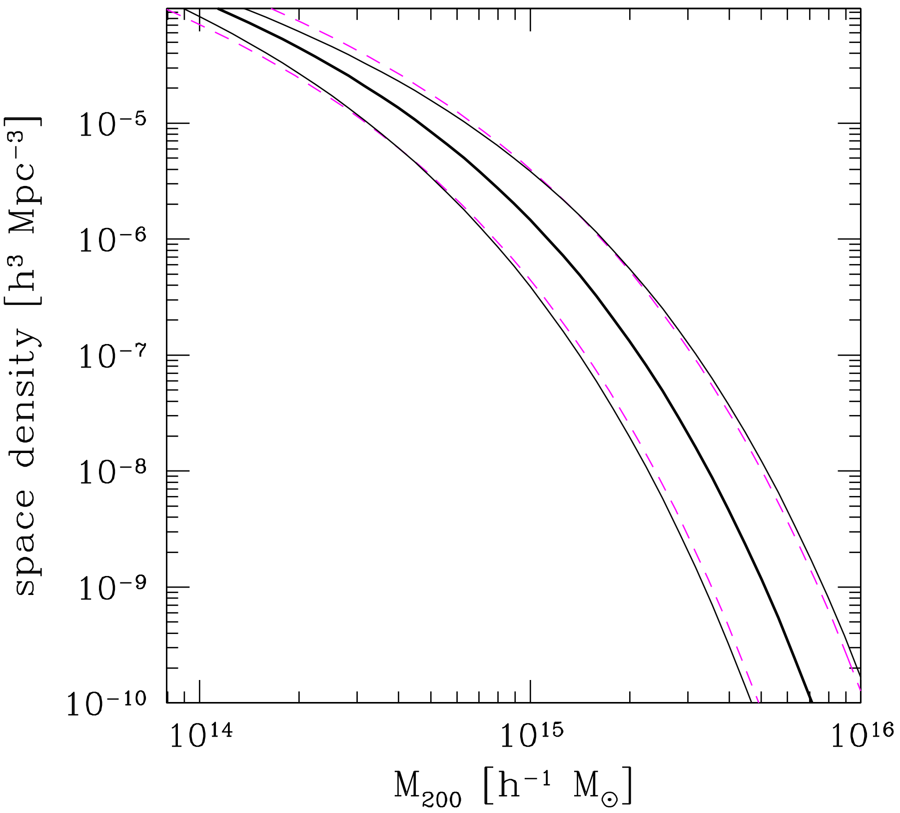

Fig. 1.4. The bold line shows the Jenkins mass function expectations for a ΛCDM cosmology with a default value $\sigma_8 = 0.9$. Solid lines to the right and left of the default give the Jenkins mass function for modified normalizations $\sigma_8 = 0.9\, e^{\pm 0.148}$. The dashed lines show the default Jenkins mass function with masses displaced by amounts $e^{\pm 0.371}$. The degeneracy between mass scale and σ_8 is apparent at space densities below $10^{-5} h^3$ Mpc^{-3}.

$H(z) = 100\, h(z)$ km s^{-1} Mpc^{-1}* is the Hubble parameter at redshift z. If ε is independent of mass and redshift (i.e., under a self-similar assumption), or is at least approximately so over some finite range, then we expect scalings of the form

$$\sigma_{\rm DM} \;=\; \sigma_{\rm DM,15}\; [h(z) M_\Delta / 10^{15} M_\odot]^{\alpha}, \tag{1.11}$$

$$kT \;=\; kT_{15}\; [h(z) M_\Delta / 10^{15} M_\odot]^{\alpha_T} \tag{1.12}$$

with slope $\alpha = \alpha_T/2 = 1/3$ and where the values of the intercepts will depend on the choice of threshold scale Δ. Note that if a mean mass measure is used, then $h(z)M_\Delta$ is replaced by $(1+z)^{3/2} M_\Delta$ (Bryan & Norman 1998).

* This term is often written with the notation $E(z) = H(z)/H_0$ used by Peebles (1993).

Table 1.2. *Empirical Mass-temperature Relations*

Reference	$M_{500}\,(6\ \mathrm{keV})$ $(10^{15}\,h^{-1}M_{\odot})$	$\mathrm{d}\ln M/\mathrm{d}\ln T$
Horner, Mushotzky, & Scharf (1999)[a]	0.40	1.78
Mohr, Mathiesen, & Evrard (1999)	0.47	1.64
Nevalainen, Markevitch, & Forman (1999)	0.17	1.79
Finoguenov, Reiprich, & Böhringer (2001)	0.30	1.85
Allen, Schmidt, & Fabian (2002)	0.39	1.54
Shimizu et al. (2003)	0.40	1.90
Sanderson et al. (2003)	0.44	1.84

[a]Isothermal model estimates.

1.3.2 Estimates of ICM Virial Scaling

Tension has developed between observational and computational estimates of the scaling between mass and ICM temperature. From X-ray observations of surface brightness and spectral temperature, one can construct the radial pressure profile of the ICM and use the assumption of strict hydrostatic equilibrium, $GM(<r)/r^2 = -\nabla P/\rho$, to derive mass estimates. This exercise has been done for samples of moderate size (many tens), and results are summarized in Table 1.2. Because T is the independent observable, fits to the inverse of Equation (1.12) are quoted, pivoted about a typical cluster temperature of 6 keV. Values of the mass intercept are defined at a critical contrast of 500, a scale accessible at moderate signal-to-noise ratio for many X-ray cluster images. In cases where a different scale is quoted, I assume an NFW profile with concentration $c = 5$ to rescale to $\Delta = 500$ (convenient expressions for this are given in an Appendix of Hu & Kravtsov 2003). Statistical errors quoted in the references are typically $\sim 10\%$ in each parameter.

The fits listed in Table 1.2 consistently indicate a slope that is steeper than the self-similar expectation $1/\alpha_T = 3/2$. With the exception of Nevalainen et al. (1999), the intercepts are in good agreement with $M_{500}\,(6\ \mathrm{keV}) = (0.40 \pm 0.05) \times 10^{15} h^{-1} M_{\odot}$.

The fact that observed scaling relations differ from self-similar predictions motivates the addition of ICM physics beyond gravitational shock heating. Voit et al. (2003) discuss the roles of radiative cooling and heating associated with galactic feedback, and focus on the gas entropy $K = kT/\rho_{\mathrm{ICM}}^{2/3}$ as the controlling parameter.

The tight color-magnitude relation of early-type cluster galaxies observed in low- to moderate-redshift clusters (Bower, Lucey, & Ellis 1992; Stanford, Eisenhart, & Dickinson 1998) implies that most of the stars in galaxies were formed at high redshifts $z \gtrsim 4$. If these galaxies hosted vigorous outflows during their rapidly star-forming phase, as appears to be the case for $z \simeq 3$ Lyman-break galaxies (e.g., Adelberger et al. 2003), then the thermal energy deposited by the outflows could raise the entropy of the surrounding intergalactic/protocluster environment. This "preheating" of the gas offers a relatively simple mechanism capable of breaking self-similarity in the ICM (Evrard & Henry 1991; Kaiser 1991).

Bialek, Evrard, & Mohr (2001) show that simulated clusters that employ an elevated initial ICM entropy at a level $K = 55 - 150\ \mathrm{keV\ cm}^{-2}$ offer an acceptable match to the local

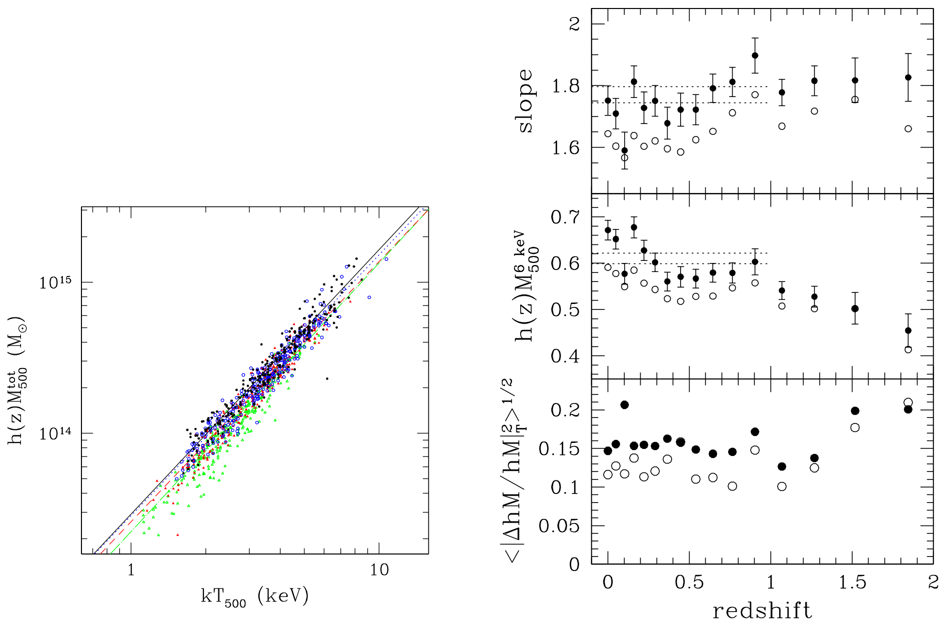

Fig. 1.5. The virial relation from a set of 68 preheated cluster simulations that match the local, observed ICM scaling relations (Bialek et al. 2001). *Left:* Virial mass $h(z)M_{500}$ against spectral temperature for redshift ranges $z < 0.2$ (filled circles), $0.2 < z < 0.5$ (open circles), $0.5 < z < 1$ (filled triangles), and $1 < z < 2$ (open triangles). *Right:* Parameters of power-law fits to these data using either spectral (filled points with error bars) or mass-weighted (open) temperatures: slope (upper panel), mass intercept $M_{500}(6\ \mathrm{keV})$ in units of $10^{15}M_\odot$ (middle panel), and rms dispersion in mass about the best-fit relation (lower panel). Dashed lines in the upper two panels show the 90% confidence range of the slope and intercept derived from a simultaneous fit to all $z < 1$ outputs.

observed scalings of ICM mass, bolometric luminosity, and isophotal size with X-ray temperature. Figure 1.5 shows the relation between virial mass and temperature for a set of 68 clusters, simulated assuming initial $K = 106$ keV cm^{-2}, at 12 epochs ranging from $z \simeq 2$ to the present. The left panel employs spectral temperatures derived from single-temperature `mekal` fits to synthetic X-ray spectra created by summing the `mekal` contributions from all gas lying within r_{500} of the cluster center. For comparing to observations, this measure of temperature is more appropriate to use than a mass-weighted measure. Low-entropy gas in the cores of infalling satellites has a larger effect when emission weighted [$\propto \rho^2 \Lambda(T)\, dV$] rather than mass weighted ($\propto \rho\, dV$). Depending on the energy passband, temperature differences at the ten percent level are expected between these two measures (Mathiesen & Evrard 2001).

The simulated cluster sample is well fit by a power law with $\sim 17\%$ scatter in mass at fixed temperature. At redshifts $z \lesssim 1$, the virial scaling under preheating is slowly evolving. A simultaneous fit to all data from these epochs, treating all outputs as independent, leads to a mean relation

Table 1.3. *Computational Mass-temperature Intercepts*

Reference	M_{500} (6 keV) ($10^{15}\,h^{-1}M_{\odot}$)
Evrard, Metzler, & Navarro (1996)	0.52
Bryan & Norman (1998)	0.78
Mathiesen & Evrard (2001)	0.83
Thomas et al. (2002)	0.40
Borgani et al. (2004)	0.43
Bialek et al. (2004)	0.61

$$h(z)M_{500} \;=\; (0.61 \pm 0.01) \left(\frac{kT}{6\,\mathrm{keV}}\right)^{1.77\pm0.02} \times 10^{15} M_{\odot}. \tag{1.13}$$

The combined effects of preheating, which affects the energetics of shallower potential wells more so than deep ones, and use of spectral instead of mass-weighted temperatures produce a slope $\mathrm{d}\ln M/\mathrm{d}\ln T$ that is $\sim 20\%$ steeper than the self-similar expectation and more consistent with the observational estimates. However, the intercept of Equation (1.13) is $\sim 50\%$ high compared to the empirical estimates.

This tension between computational and empirical determinations of the cluster mass scale appears generically true for simulations that ignore radiative cooling of the ICM. Table 1.3 lists estimates from simulated samples. The models of Thomas et al. (2002) and Borgani et al. (2004) employ radiative cooling and provide values consistent with the observed mean. The remaining models, which ignore radiative cooling, paradoxically tend to produce an ICM that is *cooler* than the radiative solution for a given mass halo. The *PdV* work done in compressing gas into regions where efficient cooling has removed gas is the mechanism that explains why "cooling causes heating" (Bryan 2000; Pearce et al. 2000).

The cooling models may relieve the tension in the ICM virial relation, but there may be a cost to this cure. The reason that the recent 2×480^3 particle GADGET-2 simulation of Borgani et al. (2004) produces a lower mass intercept is that the gas-phase structure is inverted relative to that displayed by most non-cooling simulations: the dense core gas is hotter, not cooler, than the surrounding lower density material. The inverted phase structure helps drive up the emission-weighted temperature at fixed mass, hence down the mass at 6 keV, but Borgani et al. show that the price paid is that radially averaged temperature profiles of the model clusters fall too steeply compared to observations (Markevitch 1998; DeGrandi & Molendi 2001; Pratt & Arnaud 2002). Adding transport processes such as turbulent thermal conduction (Narayan & Medvedev 2001) may help smooth the gradients, but perhaps this inclusion would then also damage agreement with observed ICM scalings.

In short, direct simulation methods are making headway and will continue to improve as the effects of coupled physical processes are sorted out. In the meantime, it is worthwhile considering a simpler approach to calibrating the ICM virial relation.

1.3.3 A "Back Door" Approach: The ICM Virial Relation from $n(T)$

Another way to constrain the mass-temperature relation is by a simple counting argument—identify the mass at which the theoretical space density of halos $n(M,z)$ matches the observed space density of clusters as a function of temperature $n(T,z)$. In practice, one needs to account for scatter by convolving

$$n(T,z)\mathrm{d}\ln T \;=\; \int \mathrm{d}\ln M\, n(M,z)\, p(T|M,z), \tag{1.14}$$

where the form of the conditional PDF $p(T|M,z)$ provides the critical link between theory and observation.

The detailed form of $p(T|M,z)$ will be set by the physical processes governing the ICM thermodynamical evolution, by the chosen mass measure, and to some degree by the assumed cosmology. Assuming for now that gravitational heating is the dominant process, then the ICM temperature should follow the depth of the dark matter potential as measured by the (one-dimensional) dark matter velocity dispersion σ_{DM}. Here ${\sigma_{\mathrm{DM}}}^2 \equiv \int dV \rho_{\mathrm{DM}} |\mathbf{v} - \bar{\mathbf{v}}|^2 / 3M_{\Delta}$ is the second moment of the fluid velocity $\mathbf{v}$ relative to the cluster mass-weighted mean $\bar{\mathbf{v}}$, and the integral is performed over the same spherical volume used to define the mass. Following the lead of Cavaliere & Fusco-Femiano (1976), introduce the parameter

$$\beta \;=\; {\sigma_{\mathrm{DM}}}^2 / (kT/\mu m_p) \tag{1.15}$$

that measures the ratio of specific energies in dark matter and ICM gas.

By wrapping our ignorance of ICM physics into the parameter β, we can proceed to pose the question of how well the virial relation for the dark matter (Eq. 1.11) is understood from simulations.

1.4 The Dark Matter Virial Relation

Calibrating the virial scaling of dark matter is a far more tractable exercise compared to that for the ICM, especially if one limits the analysis to the standard assumption of weakly interacting cold dark matter (CDM). Collisionless N-body simulations are a sufficient and mature methodology for this exercise. Still, there remains the question of whether different N-body codes will produce consistent answers in the deeply nonlinear regime.

The answer to this exercise is presented in Figures 1.6 and 1.7 and Table 1.4. The panels of Figure 1.6 show results from numerical cluster samples produced by different investigators employing five independent simulation codes (see caption for references). Clusters are identified using a critical SO(200) condition. Some methods allow the r_{200} spheres of clusters to overlap, but the center of one cannot lie within the boundary of another. In the overlap case, label the larger member of an overlapping pair the *primary* and the smaller member the *satellite*. The latter account for $5\% - 10\%$ of the population between 10^{14} and $10^{15}\, h^{-1} M_{\odot}$. As shown in panel ($a$) of Figure 1.6, the satellite population follows a slightly different virial relation from the primaries, with a distribution of σ_{DM} skewed to larger velocities. This population contains objects in the throes of ongoing mergers, and it will be ignored in the statistical analysis to follow. Their omission changes the virial relation fits at a level below one percent.

The simulation samples and the unbinned, least-squares fit parameters to Equation (1.11) are described in Table 1.4. There is a wide range in sample size and mass resolution, from Hubble Volume samples with roughly one-half million objects but only 450 particles in a

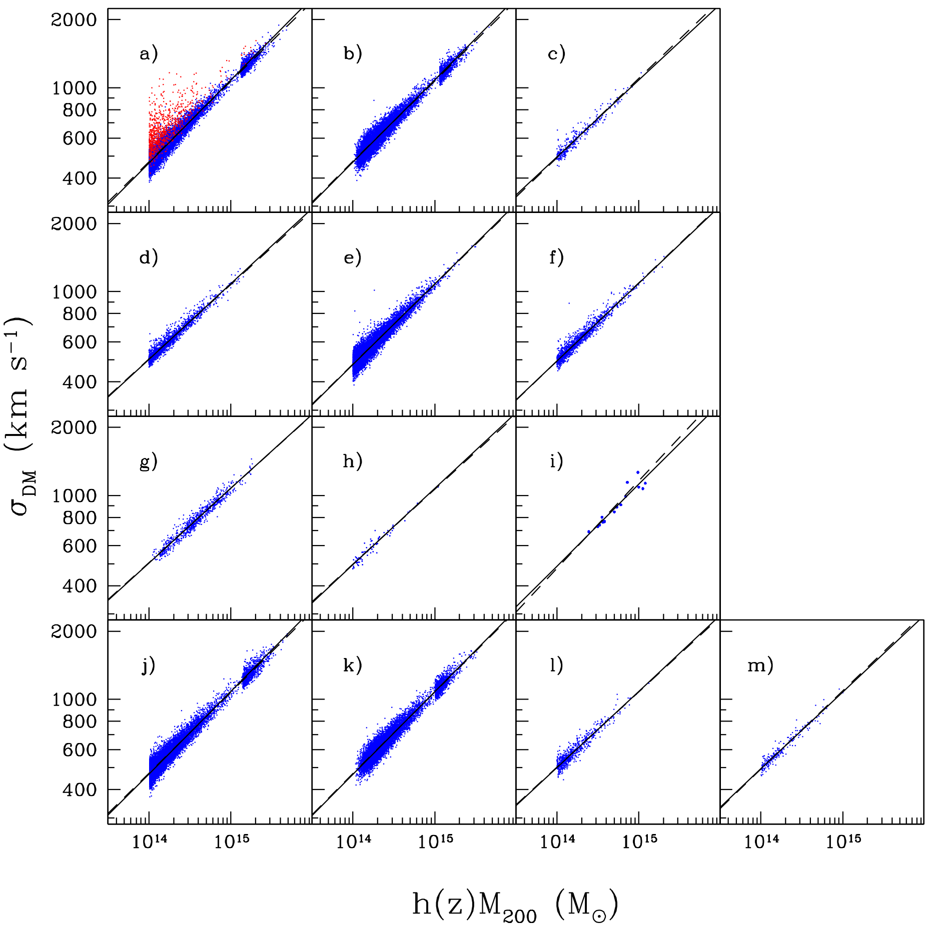

Fig. 1.6. The dark matter virial relation produced by five independent simulation codes. All panels show $z=0$ data except (*b*) and (*k*), which show sky survey data extending to $z \simeq 1.5$. For large samples, the most massive 1,000 clusters are shown along with a random sampling of 9,000 above a minimum mass of $h(z)M_{200}=10^{14}M_\odot$. Panels (*a*)–(*i*) use a ΛCDM cosmology with $\Omega_m=0.3$, $\Omega_\Lambda=0.7$ with spectrum normalizations in the range $\sigma_8 \simeq 0.8-1$. Panels (*a*)–(*f*) and (*j*)–(*m*) model only dark matter, while (*g*)–(*i*) are two-fluid simulations that include a $\sim 10\%$ baryonic mass component. Specific references are as follows: (*a*)–(*b*) Hubble Volume $z=0$ and combined sky survey samples, respectively, from Evrard et al. (2002); (*c*) Virgo model of Jenkins et al. (1998); (*d*) combined lcdm300A, 300B, 256A, 128A runs of White (2002); (*e*)–(*f*) 256^3 particle simulations of size 768 and 384 h^{-1} Mpc, respectively, from M. Warren (priv. comm.); (*g*) P3MSPH preheated ICM models of Bialek et al. (2004); (*h*) combined concordance150 SPH models from M. White (priv. comm.); (*i*) GADGET SPH models of Rasia, Tormen & Moscardini (2004); (*j*)–(*k*) τCDM ($\Omega_m=1$) Hubble Volume $z=0$ and combined sky survey samples, respectively, from Evrard et al. (2002); (*l*) τCDM Virgo model of Jenkins et al. (1998); (*m*) open CDM ($\Omega_m=0.3$) from M. White (priv. comm.). Points in each panel show primary cluster data (except for panel *a*, which shows both primary and satellites; see text for definition), while the solid and dashed lines are fits using no binning and binning primary data in intervals of 0.1 in decimal $\log[h(z)M_{200}]$, respectively. Parameter values of the former are listed in Table 1.4.

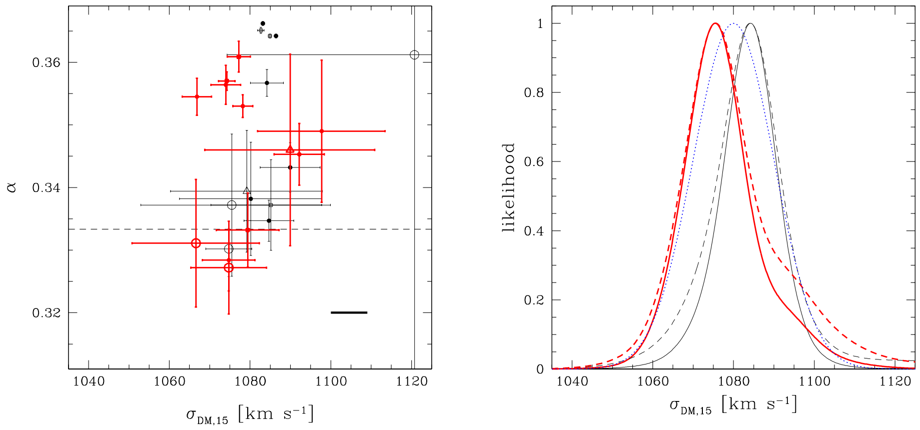

Fig. 1.7. *Left:* Fit parameters of the dark matter virial relation (Eq. 1.11) derived from log-linear, least-squares fits using equal weight per data point (thin lines) or equal weight for points binned in intervals of 0.1 in decimal $\log[h(z)M_{200}]$ (bold lines). The dashed line marks a self-similar slope of $1/3$, and the bar denotes a systematic uncertainty of 0.5% in $\sigma_{\rm DM}$, a conservative estimate of the energy conservation accuracy of most codes. Filled symbols are pure N-body, while open include gas. Circles are ΛCDM, squares τCDM and triangles OCDM. *Right:* Likelihood estimates of the intercept $\sigma_{\rm DM,15}$ derived by combining the log-normal PDFs of all the models using inverse variance (solid) or equal weighting (dashed), and for unbinned (light) or binned (bold) fits. The dotted line shows the summary result, Equation (1.16).

Coma-like cluster to a sample of 16 individual cluster simulations with nearly 1000 times improved mass resolution. Samples cover three cosmologies, epochs in the range $z \lesssim 1.5$, and three sets include a baryonic component gravitationally coupled to the dark matter.

The left panel of Figure 1.7 shows that there is remarkably good agreement in the dark matter virial relation fits among the samples. The slope is not particularly well determined, and tends to be somewhat steeper than the self-similar expectation of $1/3$. But the intercept $\sigma_{\rm DM,15}$ is defined remarkably well. The statistical error in the very large Hubble Volume samples is extremely small (0.03%), much smaller than the typical energy accuracy ($\lesssim 1\%$) of the time integration schemes employed by N-body codes.

The right panel of Figure 1.7 shows estimates of $\sigma_{\rm DM,15}$ based on summing log-normal PDFs from each sample fit, using either inverse variance weighting (solid) or linear weighting (dashed). To account for integration error, an uncertainty of 0.5% is added in quadrature to the statistical error in $\sigma_{\rm DM}$. The resultant PDFs are reassuringly insensitive to the weighting scheme employed, but there is a slight shift between the binned (median 1077 km s^{-1}) and unbinned (median 1084 km s^{-1}) results. A Gaussian with mean and dispersion

$$\sigma_{\rm DM,15} \ = \ 1080 \pm 10 \, {\rm km \ s}^{-1} \tag{1.16}$$

has a 90% confidence range that overlaps the estimates for both approaches. The uncertainty of 10 km s^{-1}, a one percent calibration of $\sigma_{\rm DM,15}$, signals a high level of integrity in N-body solutions of strongly nonlinear clustering.

Table 1.4. *Dark Matter Virial Relation Calibrations*

Panel[a]	$N_{\rm cl}^{b}$	N_{15}^{c}	$\sigma_{\rm DM,15}{}^{d}$	Slope[d]
(*a*)	581866	450	1083.3 ± 0.3	0.3662 ± 0.0002
(*b*)	494803	450	1086.4 ± 0.3	0.3642 ± 0.0002
(*c*)	355	14,660	1080 ± 11	0.338 ± 0.006
(*d*)	1699	~ 100000	1085 ± 4	0.335 ± 0.002
(*e*)	8936	450	1084 ± 2	0.357 ± 0.001
(*f*)	1461	3400	1090 ± 5	0.343 ± 0.002
(*g*)	777	~ 15000	1075 ± 3	0.330 ± 0.003
(*h*)	158	~ 25000	1075 ± 14	0.337 ± 0.007
(*i*)	16	~ 300000	1121 ± 28	0.361 ± 0.032
(*j*)	601942	450	1085.6 ± 0.2	0.3642 ± 0.0002
(*k*)	263019	450	1083.7 ± 0.5	0.3651 ± 0.0003
(*l*)	703	4400	1085 ± 9	0.337 ± 0.004
(*m*)	221	~ 60000	1079 ± 11	0.339 ± 0.006

[a] Fig. 1.6.
[b] Number of clusters in sample.
[c] Number of particles in a $10^{15}\,h^{-1}M_\odot$ cluster.
[d] Quoted uncertainties are statistical.

1.5 Interpreting $n(T)$: An Example of Cosmological-Astrophysical Confusion

With well calibrated forms for the mass function and dark matter virial relations, the space density of dark matter potential wells can be accurately predicted from the linear fluctuation spectrum $\sigma(M)$. The β parameter then maps this distribution to an observable space density of temperature $n(T)$.

For a ΛCDM model with $\Omega_{\rm m} = 0.3$ and $\sigma_8 = 0.9$, Evrard et al. (2002) show that $\beta = 0.92 \pm 0.06$ provides a good match to the combined observational samples of Markevitch (1998) and White (2000) that were employed in the σ_8 analysis of Pierpaoli, Scott, & White (2001). The quoted uncertainty in β is due to shot noise in the relatively small sample, which contains ~ 20 clusters hotter than 6 keV.

The mass normalization implied by combining $\beta = 0.92$ with the dark matter virial calibration is $M_{500}(6\ {\rm keV}) = 0.49 \times 10^{15}\,h^{-1}M_\odot$ (assuming a $c = 5$ NFW profile for which $M_{200} = 1.38 M_{500}$). This value is appropriate for the assumed normalization $\sigma_8 = 0.9$. If a slightly different value of σ_8 had been chosen, then the mass scale at fixed space density would shift by an amount $d\ln M = 2.5\, d\ln\sigma_8$ (Fig. 1.4) across the entire observed range. Since the space density at a given temperature is fixed by the observations, the mass-temperature intercept required for the model to match the data will scale as

$$M_{500}(6\ {\rm keV}) \ = \ (0.64 \pm 0.06)\,\sigma_8{}^{5/2} \times 10^{15}\,h^{-1}M_\odot. \tag{1.17}$$

This can be alternately expressed as a constraint on the characteristic temperature (for $\Delta = 500$ in Eq. 1.12)

$$kT_{15} \ = \ (8.1 \pm 0.5)\,\sigma_8{}^{-5/3}\ {\rm keV} \tag{1.18}$$

or on the ratio of specific energies

$$\beta = (1.10 \pm 0.07)\, {\sigma_8}^{5/3}. \tag{1.19}$$

These relations all assume a fixed *shape* of the linear power spectrum, appropriate for a $\Omega_{\rm m}=0.3$ Universe. As $\Omega_{\rm m}$ is varied, the mass function tilts, with lower values of $\Omega_{\rm m}$ leading to flatter $n(M)$ and *vice versa*. The matter density is therefore mainly degenerate with the slope of the mass-temperature relation, but there is a normalization effect as well. The cumulative space density of clusters more massive than $\sim 10^{14.5}\, h^{-1} M_{\odot}$ is sensitive to the parameter combination $\sigma_8 \Omega_{\rm m}^{0.6}$ (Pierpaoli et al. 2001). Roughly speaking, we can generalize the argument above by replacing σ_8 with $\sigma_8(\Omega_{\rm m}/0.3)^{0.6}$. A more careful approach would examine the full likelihood surface in the space of $\{\sigma_8, \Omega_{\rm m}, kT_{15}, \alpha_T\}$, but this remains to be done.

1.5.1 A Cluster Energetics Problem?

Under the assumption that the principal mechanism of ICM heating is through gravitationally induced shocks, existing gas dynamic simulations are able to provide an independent constraint on the specific energy ratio β. The shock-heating efficiency for this case is well calibrated by a set of 12 largely independent simulations of a single cluster (the "Santa Barbara" cluster of Frenk et al. 1999). The ensemble mean of the simulations is

$$\beta_{\rm sim} = 1.17 \pm 0.05. \tag{1.20}$$

A value greater than unity reflects incomplete thermalization of the ICM; the gas is partly supported by kinetic pressure of large-scale turbulent motions (Evrard 1990; Navarro et al. 1995; Rasia et al. 2004). When compared to the value derived from the space density argument (Eq. 1.19), we infer that $\sigma_8=1.06 \pm 0.05$ is required for an ΛCDM model with $\Omega_{\rm m}=0.3$.

Such a high value of σ_8 has fallen out of favor recently. Analysis of microwave background anisotropies from the *WMAP* mission (Spergel et al. 2003) yields $\sigma_8=0.90 \pm 0.1$ for an ΛCDM model with $\Omega_{\rm m}=(0.29 \pm 0.04)(h/0.7)^2$ and a power-law primordial fluctuation spectrum with $n_s = 1$. When other CMB and large-scale structure data (2dF galaxy survey and Lyα forest observations) are added to the analysis of this model, the spectrum normalization drops to $\sigma_8=0.75^{+0.08}_{-0.07}$, while the matter density constraint is essentially unchanged.

There is a $\sim 3\sigma$ difference between this low value of σ_8 and the value derived from the cluster $n(T)$ argument above. What is wrong if σ_8 drops to 0.75? Well, lower σ_8 models make fewer massive clusters, so matching the observed space density of hot clusters requires lowering the β parameter to

$$\beta_{\rm WMAP} = 0.68 \pm 0.12. \tag{1.21}$$

Since the relation between $\sigma_{\rm DM}$ and mass is now fixed at the percent level, the only way to decrease β is to increase the ICM temperature at fixed mass. Relative to the case of purely gravitational heating, the boost in temperature required to match the lower *WMAP* normalization result would be

$$\frac{kT_{\rm WMAP}}{kT_{\rm grav}} = \frac{\beta_{\rm sim}}{\beta_{\rm WMAP}} = 1.72 \pm 0.30. \tag{1.22}$$

The extra energy, 0.7 ± 0.3 of that produced by gravity, is very large, $\sim 10^{63}$ erg for the Coma cluster. To put this number in perspective, assume that the stellar mass in galaxies, $M_{\rm gal}$, is one-tenth the ICM mass (Lin, Mohr, & Stanford 2003). Then the overall stellar/black hole energy feedback efficiency (fraction of $M_{\rm gal}c^2$) required to provide the extra ICM heat is $\sim 10^{-4}(kT/6\,{\rm keV})$. It is not at all clear whether the combined actions of known heating sources such as supermassive black hole-driven bubbles and supernova-driven winds, can produce an efficiency as large as this.

In addition, it is worth considering the other observable tracer of potential well depth, the galaxy velocity dispersion $\sigma_{\rm gal}$. The ratio $\beta_{\rm gal} \equiv \sigma_{\rm gal}/(kT/\mu m_p)$ for clusters is measured to be 1.0 ± 0.1 (e.g., Xue & Wu 2000). The ratio of galaxy to dark matter specific energies is then

$$\left(\frac{\sigma_{\rm gal}}{\sigma_{\rm DM}}\right)^2 = \frac{\beta_{\rm gal}}{(1.10 \pm 0.07)\sigma_8{}^{5/3}} = 1.47 \pm 0.26 \tag{1.23}$$

for the *WMAP* plus large-scale structure normalization. Apparently, galaxies, like the ICM, must end up hotter than the dark matter. Simulations of galaxy formation within clusters generally find the opposite; bright galaxies are slightly cooler than the mass (Springel et al. 2001).

Might this be an indication of new physics involving dark matter cooling? Perhaps, but this may be overreacting to what is now only a 3σ result. There may be more mundane explanations, especially if σ_8 relaxes upward. One possibility is that the temperatures determined from X-ray spectra are biased high relative to mass-weighted values, but deprojected cluster profiles do not support this idea (Allen et al. 2002), and simulations suggest that the effect works in the opposite direction (Mathiesen & Evrard 2001). Another possibility is that a number of smaller effects combine to produce the net offset. Three sources of $\sim 20\%$ bias could do the job, for example. Such a conspiratorial explanation has historical precedent in the original "beta-discrepancy" (Evrard 1990), where three reinforcing effects explain why values of $\beta_{\rm gal}$ are typically $\sim 50\%$ larger than values estimated from X-ray image profiles.

1.6 Discussion

The impressions I am trying to convey in this article are: (1) the statistical character of nonlinear structure is now very well established by simulations, and a population of structurally regular dark matter halos is expected at all redshifts; (2) a sound framework for extracting cosmological parameters from cluster surveys is thus in place; but (3) accurate constraints from such surveys demand a firm understanding of how observables relate to dark matter (along with, of course, a careful treatment of survey systematics).

The exercise of determining the power spectrum normalization σ_8 through the temperature space density $n(T)$ of clusters affords an example of astrophysical/cosmological confusion. Current observations place the constraint $\beta/\sigma_8{}^{5/3} = 1.10 \pm 0.07$ on an $\Omega_{\rm m} = 0.3$ ΛCDM Universe. A normalization as low as $\sigma_8 = 0.75$ implies the existence of significant extra heat input to the ICM and/or new sources of bias in spectroscopic analysis of X-ray emission.

The era of large-N (10,000 or more) cluster samples is on the horizon. In the optical, the SDSS (Bahcall et al. 2003), 2dF (Couch, Colless, & De Propris 2004), and 2MASS (Kochanek et al. 2003) surveys will cover low redhifts, while the RCS2 (Gladders 2004) and other deep surveys will push beyond $z \approx 1$. In the X-rays, the XMM Cluster Survey (Romer et al. 2001) will identify large numbers of intermediate-redshift clusters with $T_{\rm X} \gtrsim 4$ keV. The deepest reach will come from upcoming Sunyaev-Zel'dovich surveys (Holder et al. 2000; Kneissl et al. 2001; Carlstrom et al. 2002).

Theorists are gearing up to handle the data deluge. Survey design is guided by understanding the trade-offs in sample and shot noise errors (Hu & Kravtsov 2003). Projection and selection effects can be quantified using mock catalogs constructed from N-body simulations (Wechsler et al. 2004). The notion that surveys can be "self-calibrated" to non-standard astrophysical evolution (Majumdar & Mohr 2002; Hu 2003) is reinforcing optimism that the upcoming large cluster samples will constrain the equation of state parameter of the dark energy at the 10%-level or better (Haiman, Mohr, & Holder 2001; Molnar, Birkinshaw, & Mushotzky 2002; Weller, Battye, & Kneissl 2002).

Regardless of whether such parameter estimation forecasts are actually met, the next few decades promise to be a very exciting period for cosmology and galaxy cluster astrophysics.

Acknowledgements. Many thanks to John, Alan and (the other) Gus for putting together an outstanding program. I am grateful for their (and Luis Ho's) extreme patience in awaiting this contribution to the proceedings. Thanks also to my collaborators—John Bialek, Joe Mohr, Risa Wechsler, Martin White, Elena Rasia, Giuseppe Tormen, Lauro Moscardini, Mike Warren, Salmon Habib, Katrin Heitmann and members of the Virgo Consortium—for allowing me to present results of ongoing studies. This research is supported by the NSF and by NASA.

References

Adelberger, K. L., Steidel, C. C., Shapley, A. E., & Pettini, M. 2003, ApJ, 584, 45
Allen, S. W., Schmidt, R. W., & Fabian, A. C. 2002, MNRAS, 334, L11
Bahcall, N. A., & Fan, X. 1998, ApJ, 504, 1
Bahcall, N. A., et al. 2003, ApJS, 148, 243
Bennett, C. L., et al. 2003, ApJS, 148, 1
Bernardeau, F., Colombi, S., Gaztanaga, E., & Scoccimarro, R. 2002, Phys. Rep., 367, 1
Bertschinger, E. 1985, ApJS, 58, 39
——. 1998, ARA&A, 36, 599
Bialek, J., et al. 2004, in preparation
Bialek, J., Evrard, A. E., & Mohr, J. J. 2001, ApJ, 555, 597
Bode, P., Bahcall, N. A., Ford, E. B., & Ostriker, J. P. 2001, ApJ, 551, 15
Bond, J. R., Cole, S., Efstathiou, G., & Kaiser, N. 1991, ApJ, 379, 440
Bond, J. R., & Efstathiou, G. 1984, ApJ, 285, L45
Bond, J. R., Kofman, L., & Pogosyan, D. 1996, Nature, 380, 603
Borgani, S., et al. 2001, ApJ, 561, 13
——. 2004, MNRAS, in press (astro-ph/0310794)
Borgani, S., Girardi, M., Carlberg, R. G., Yee, H. K. C., & Ellingson, E. 1999, ApJ, 527, 561
Bower, R. G. 1991, MNRAS, 24, 332
Bower, R. G., Lucey, J. R., & Ellis, R. S. 1992, MNRAS, 254, 589
Briel, U. G., Henry, J. P., & Böhringer, H. 1992, A&A259, L31
Brüggen, M., & Kaiser, C. R. 2002, Nature, 418, 301
Bryan, G. L. 2000, ApJ, 544, L1
Bryan, G. L., & Norman, M. L. 1998, ApJ, 495, 80
Carlstrom, J. E., Holder, G. P., & Reese, E. D. 2002, ARA&A, 40, 643
Carroll, S. M., Press, W. H., & Turner, E. L. 1992, ARA&A, 30, 499
Cavaliere, A., & Fusco-Femiano, R. 1976, A&A, 49, 137
Cole, S., Lacey, C. G., Baugh, C. M., & Frenk, C. S. 2000, MNRAS, 319, 168
Couch, W. J., Colless, M. M., & De Propris, R. 2004, in Carnegie Observatories Astrophysics Series, Vol. 3: Clusters of Galaxies: Probes of Cosmological Structure and Galaxy Evolution, ed. J. S. Mulchaey, A. Dressler, & A. Oemler (Cambridge: Cambridge Univ. Press), in press
Davis, M., Efstathiou, G., Frenk, C. S., & White, S. D. M. 1985, ApJ, 292, 371
De Grandi, S., & Molendi, S. 2001, ApJ, 551, 153
Dressler, A. 1978, ApJ, 226, 55
Donahue, M., Voit, G. M., Gioa, I. M., Luppino, G., Hughes, J. P., & Stocke, J. T. 1998, ApJ, 502, 550

Efstathiou, G., Frenk, C. S., White, S. D. M., & Davis, M. 1988, MNRAS, 235, 715
Eke, V. R., Cole, S., & Frenk, C. S. 1996, MNRAS, 282, 263
Evrard, A. E. 1989, ApJ, 341, L71
——. 1990, ApJ, 363, 34
Evrard, A. E., et al. 2002, ApJ, 573, 7
Evrard, A. E., & Gioia, I. M. 2002, in Merging Processes in Galaxy Clusters, ed. L. Ferretti, I. M. Gioia, & G. Giovannini (Dodrecht: Kluwer), 253
Evrard, A. E., & Henry J. P. 1991, ApJ, 383, 95
Evrard, A. E., Metzler, C., & Navarro, J. F. 1996, ApJ, 469, 494
Finoguenov, A., Reiprich, T. H., & Böhringer, H. 2001, A&A, 368, 749
Frenk, C. S., et al. 1999, ApJ, 525, 554
Girardi, M., Borgani, S., Giuricin, G., Mardirossian, F., & Mezzetti, M. 2000, ApJ, 530, 62
Gladders, M. D. 2004, in Carnegie Observatories Astrophysics Series, Vol. 3: Clusters of Galaxies: Probes of Cosmological Structure and Galaxy Evolution, ed. J. S. Mulchaey, A. Dressler, & A. Oemler (Cambridge: Cambridge Univ. Press), in press
Governato, F., Babul, A., Quinn, T., Tozzi, P., Baugh, C. M., Katz, N., & Lake, G. 1999, MNRAS, 307, 949
Gunn, J. E., & Gott, J. R. 1972, ApJ, 176, 1
Haiman, Z., Mohr, J. J., & Holder, G. P. 2001, ApJ, 553, 545
Holder, G. P., Mohr, J. J., Carlstrom, J. E., Evrard, A. E., & Leitch, E. M. 2000, ApJ, 544, 629
Horner, D. J., Mushotzky, R. F., & Scharf, C. A. 1999, ApJ, 520, 78
Hu, W. 2003, Phys. Rev. D, 67, 081304
Hu, W., & Kravtsov, A. V. 2003, ApJ, 584, 702
Jenkins, A., et al. 1998, ApJ, 499, 20
Jenkins, A., Frenk, C. S., White, S. D. M., Colberg, J. M., Cole, S., Evrard, A. E., Couchman, H. M. P., & Yoshida, N. 2001, MNRAS, 321, 372
Kaiser N. 1986, MNRAS, 222, 323
——. 1991, ApJ, 383, 104
Kauffmann, G., Colberg, J. M., Diaferio, A., & White, S. D. M. 1999, MNRAS, 303, 188
Kneissl, R., Jones, M. E., Saunders, R., Eke, V. R., Lasenby, A. N., Grainge, K., & Cotter, G. 2001, MNRAS 328, 783
Kochanek, C. S., White, M., Huchra, J., Macri, L., Jarrett, T. H., Schneider, S. E., & Mader, J. 2003, ApJ, 585, 161
Kolb, E. W., & Turner, M. S. 1990, The Early Universe (Redwood City: Addison Wesley)
Lacey, C., & Cole, S. 1994, MNRAS, 271, 676
Lin, Y.-T., Mohr, J. J., & Stanford, S. A. 2003, ApJ, 591, 749
Lokas, E. L., & Hoffman, Y. 2000, ApJ, 542, L139
Majumdar, S., & Mohr, J. J. 2003, ApJ, 585, 603
Markevitch, M. 1998, ApJ, 504, 27
Mathiesen, B. F., & Evrard, A. E. 2001, ApJ, 546, 100
Mohr, J. J., Mathiesen, B., & Evrard, A. E. 1999, ApJ, 517, 627
Molnar, S. M., Birkinshaw, M., & Mushotzky, R. F. 2002, 570, 1
Narayan, R., & Medvedev, M. V. 2001, ApJ, 562, L129
Navarro, J. F., Frenk, C. S., & White, S. D. M. 1995, MNRAS, 275, 720
Nevalainen, J., Markevitch, M., & Forman, W. 1999, ApJ, 536, 73
Nichol, R. C. 2004, in Carnegie Observatories Astrophysics Series, Vol. 3: Clusters of Galaxies: Probes of Cosmological Structure and Galaxy Evolution, ed. J. S. Mulchaey, A. Dressler, & A. Oemler (Cambridge: Cambridge Univ. Press), in press
Pearce, F. R., Thomas, P. A., Couchman, H. M. P., & Edge, A. C. 2000, MNRAS, 317, 1029
Peebles, P. J. E. 1970, AJ, 75, 13
——. 1980, in The Large Scale Structure of the Universe (Princeton: Princeton Univ. Press)
——. 1993, in Principles of Physical Cosmology (Princeton: Princeton Univ. Press)
Pierpaoli, E., Scott, D., & White, M. 2001, MNRAS, 325, 77
Pratt, G. W., & Arnaud, M. 2002, A&A, 394, 375
Press, W. H., & Schechter, P. 1974, ApJ187, 425
Rasia, E., Tormen, G., & Moscardini, L. 2004, MNRAS, in press (astro-ph/0309405)
Reed, D., Gardner, J., Quinn, T., Stadel, J., Fardal, M., Lake, G., & Governato, F. 2003, MNRAS, 346, 565
Ricker, P. M., & Sarazin, C. L. 2002, AJ, 561, 621
Roettiger, K., Burns, J. O., & Loken, C. 1996, ApJ, 473, 651

Romer, A. K., Viana, P. T. P., Liddle, A. R., & Mann, R. G. 2001, ApJ, 547, 594
Rosati, P., Borgani, S., & Norman, C. 2002, ARA&A, 40, 539
Sanderson, A. J. R., Ponman, T. J., Finoguenov, A., Lloyd-Davies, E. J., & Markevitch, M. 2003, MNRAS, 340, 989
Scott, D., Silk, J., & White, M. 1995, Science, 268, 829
Seljak, U., & Zaldarriaga, M. 1996, ApJ, 469, 437
Sheth, R. K., Mo, H. J., & Tormen, G. 2001, MNRAS, 323, 1
Sheth, R. K., & Tormen, G. 1999, MNRAS, 308, 119
Shimizu, M., Kitayama, T., Sasaki, S., & Suto, Y. 2003, ApJ, 590, 197
Somerville, R. S., & Primack, J. R. 1999, MNRAS, 310, 1087
Spergel, D. N., et al. 2003, ApJS, 148, 175
Springel, V., White, S. D. M, Tormen, G., & Kauffmann, G. 2001, MNRAS, 328, 76
Stanford, S. A., Eisenhardt, P., & Dickinson, M. 1998, ApJ, 492, 461
Szapudi, I., Colombi, S., Jenkins, A., & Colberg, J. 2000, MNRAS, 313, 725
Thomas, P. A., Muanwong, O., Kay, S. T., & Liddle, A. R. 2002, MNRAS, 330, L48
Voit, G. M., Balogh, M. L., Bower, R. G., Lacey, C. G., & Bryan, G. L. 2003, ApJ, 593, 272
Wecshler, R. H., et al. 2004, in preparation
Weller, J., Battye, R. A., & Kneissl, R. 2002, Phys. Rev. Lett., 88, 1301
White, D. A. 2000, MNRAS, 312, 663
White, M. 2001, A&A, 367, 27
——. 2002, ApJS, 143, 241
White, S. D. M., Navarro, J. F., Evrard, A. E., & Frenk, C. S. 1993, Nature, 366, 429
Xue, Y.-J., & Wu, X.-P. 2000, ApJ, 538, 65
Zwicky, F. 1933, Helv. Phys. Acta, 6, 110
——. 1937, ApJ, 86, 217